Gurdip Daffu,[1] Xiaoping Shen,[1] Laura Senatus,[1] Devi Thiagarajan,[1] Andisheh Abedini,[1] Carmen Hurtado del Pozo,[1] Rosa Rosario,[1] Fei Song,[1] Richard A. Friedman,[2] Ravichandran Ramasamy,[1] and Ann Marie Schmidt[1]

RAGE Suppresses ABCG1-Mediated Macrophage Cholesterol Efflux in Diabetes

Diabetes 2015;64:4046–4060 | DOI: 10.2337/db15-0575

Diabetes exacerbates cardiovascular disease, at least in part through suppression of macrophage cholesterol efflux and levels of the cholesterol transporters ATP binding cassette transporter A1 (ABCA1) and ABCG1. The receptor for advanced glycation end products (RAGE) is highly expressed in human and murine diabetic atherosclerotic plaques, particularly in macrophages. We tested the hypothesis that RAGE suppresses macrophage cholesterol efflux and probed the mechanisms by which RAGE downregulates *ABCA1* and *ABCG1*. Macrophage cholesterol efflux to apolipoprotein A1 and HDL and reverse cholesterol transport to plasma, liver, and feces were reduced in diabetic macrophages through RAGE. In vitro, RAGE ligands suppressed *ABCG1* and *ABCA1* promoter luciferase activity and transcription of *ABCG1* and *ABCA1* through peroxisome proliferator–activated receptor-γ (PPARG)–responsive promoter elements but not through liver X receptor elements. Plasma levels of HDL were reduced in diabetic mice in a RAGE-dependent manner. Laser capture microdissected CD68$^+$ macrophages from atherosclerotic plaques of *Ldlr*$^{-/-}$ mice devoid of *Ager* (RAGE) displayed higher levels of *Abca1*, *Abcg1*, and *Pparg* mRNA transcripts versus *Ager*-expressing *Ldlr*$^{-/-}$ mice independently of glycemia or plasma levels of total cholesterol and triglycerides. Antagonism of RAGE may fill an important therapeutic gap in the treatment of diabetic macrovascular complications.

Accelerated atherosclerosis is a leading cause of morbidity and mortality in type 1 and 2 diabetes (1,2). Important roles for accelerated vascular inflammation have been demonstrated in diabetic atherosclerosis in human and animal subjects. In particular, increased numbers of macrophages together with proinflammatory ligands of the receptor for advanced glycation end products (RAGE) populate human atherosclerotic lesions, especially in diabetes (3).

In human diabetes, serum cholesterol efflux capacity and reverse cholesterol transport (RCT) are impaired (4,5) and are mirrored in animal models of diabetes (6). The overall importance of these mechanisms is inferred from the inverse relationship between cholesterol efflux capacity and both carotid-intima thickness (7), a surrogate marker of atherosclerosis at least in human subjects without diabetes, and incident cardiovascular events (8), underscoring the relevance of HDL function to atheroprotective mechanisms. In human subjects with diabetes, macrophage levels of two key cholesterol transporters, ATP binding cassette transporter A1 (ABCA1) and ABCG1, are reduced, contributing to increased macrophage cholesterol accumulation (9,10). Despite the importance of these processes to vascular homeostasis, the precise mechanisms underlying these observations in diabetes are not delineated.

Advanced glycation end products (AGEs) form through the nonenzymatic glycation and oxidation of proteins and lipids. AGEs accumulate in diabetic plasma and tissues. One of the principal means by which AGEs exert their pathological effects is through ligation of RAGE. RAGE and their ligands AGEs, S100/calgranulins, and high-mobility group box 1 (HMGB1) are highly expressed in human and murine diabetic atherosclerotic lesions and colocalize, at least in part, with macrophage markers (11). In animal models, global deletion of *Ager* or administration of soluble RAGE (sRAGE), the RAGE ligand decoy that binds to and

[1]Diabetes Research Program, Division of Endocrinology, Department of Medicine, New York University School of Medicine, New York, NY
[2]Biomedical Informatics Shared Resource, Herbert Irving Comprehensive Cancer Center, and Department of Biomedical Informatics, College of Physicians and Surgeons, Columbia University, New York, NY
Corresponding author: Ann Marie Schmidt, annmarie.schmidt@nyumc.org.
Received 29 April 2015 and accepted 23 July 2015.
This article contains Supplementary Data online at http://diabetes.diabetesjournals.org/lookup/suppl/doi:10.2337/db15-0575/-/DC1.
G.D. and X.S. contributed equally to this work.

See accompanying article, p. 3981.

sequesters RAGE ligands, thereby inhibiting their ability to engage cell surface RAGE, is strongly protective against acceleration of diabetic atherosclerosis partly through a reduction in lesional macrophage content and vascular inflammation (12–15). Furthermore, bone marrow transplantation experiments have affirmed important roles for *Ager* expression in myeloid cells in the progression of atherosclerosis in murine models (14). In the current study, we tested the hypothesis that RAGE contributes to impaired macrophage cholesterol efflux and RCT, particularly in the RAGE ligand–enriched environment of diabetes.

RESEARCH DESIGN AND METHODS

Reagents

The following materials were purchased: apolipoprotein A1 (apoA1), HDL, and acetylated LDL (Biomedical Technologies, Inc.); fatty acid–free BSA (Equitech-Bio); T 0901317 (Tocris Bioscience); human plasma LDL (Sigma-Aldrich); assays for measurements of HDL, total cholesterol, and triglycerides (Wako Diagnostics); rosiglitazone (Sigma-Aldrich); and U0126 and PD98509 (Cell Signaling).

Animal Studies

Male homozygous $Ager^{-/-}$ (RAGE) mice (C57BL/6 $Ager^{-/-}$ mice backcrossed >12 generations into C57BL/6J [The Jackson Laboratory]) and littermate *Ager*-expressing control mice were used. Male mice (wild type [WT] and devoid of *Ager*) were rendered diabetic with streptozotocin (STZ) (Sigma-Aldrich). For high-fat diet (HFD) and low-fat diet (LFD) experiments, mice at the age of 6–8 weeks were fed HFD with 60% of calories from lard (D12492; Research Diets, Inc.) or LFD with 13% of calories from fat (5053, PicoLab Rodent Diet 20; LabDiet) for at least 3 months. $Ldlr^{-/-}$ mice devoid of or expressing *Ager* were rendered diabetic at age 7 weeks and then placed on a Western diet (0.15% cholesterol) (D01061401C; Research Diets, Inc.) for 15 weeks followed by harvest of the aortic arches at age 22 weeks. All animal procedures were approved by the Institutional Animal Care and Use Committees of Columbia University and New York University (NYU) and performed in accordance with the National Institutes of Health animal care guidelines.

Cell Culture

Human THP-1 peripheral blood monocytic cells, L929 cells, and human embryonic kidney (HEK) 293T cells were obtained from ATCC and cultured per the manufacturer's instructions. THP-1 cells were used as suspension cells throughout this study.

Isolation of Murine Macrophages

For primary murine bone marrow–derived macrophages (BMDMs), bone marrow was retrieved after kill from bilateral femora, and BMDMs were cultured as previously described (16) and used on day 7 of incubation. BMDMs retrieved from nondiabetic mice were subsequently grown in 5.5 mmol/L D-glucose, and BMDMs retrieved from diabetic mice were grown in 25 mmol/L D-glucose to mimic their condition of origin. In other studies, BMDMs from nondiabetic mice were cultured in 5.5 or 25 mmol/L D-glucose for 7 days postisolation and before studies. Peritoneal macrophages were isolated as previously described without the use of thioglycollate (17).

RNA Isolation and Quantitative Real-Time PCR

Quantitative real-time PCR was performed on isolated RNA using TaqMan Fast Universal Master Mix (2X) with premade primer sets (Life Technologies) (Supplementary Table 1).

RNA Interference Silencing

Small interfering RNA (siRNA) to reduce levels of *AGER* (ID# 110857; sense [5′–3′: CGGCUGGUGUUCCAAUAAtt] and antisense [5′–3′: UUAUUGGGAACACCAGCCGtg]) and scramble negative control siRNA (ID# AM435) were purchased from Life Technologies.

Overexpression of Peroxisome Proliferator–Activated Receptor-γ and ABCG1 in THP-1 Cells

Human peroxisome proliferator–activated receptor-γ (*PPARG*) cDNA cloned into pCMV-SPORT6 plasmid was obtained from Thermo Scientific, and human *ABCG1* cDNA cloned into pCMV6-AC-GFP plasmid was purchased from OriGene.

Cholesterol Efflux Assays

Primary murine BMDMs or THP-1 cells were labeled with 5 μCi/mL ^{3}H-cholesterol (Perkin Elmer) in the presence of acetylated LDL (50 mg/L) and fatty acid–free BSA (1%) for 24 h. After washing the cells and achieving equilibrium for 1 h with fatty acid–free BSA (1%), cells were treated with either apoA1 or HDL. After 6 h of incubation at 37°C, the supernatant was collected. Cells were washed and lysed; aliquots of both supernatant and medium were measured in a multipurpose scintillation counter (LS6500; Beckman Coulter). The percent cholesterol efflux was calculated by dividing the radioactivity in the supernatant by the sum of the radioactivity measured in the supernatant and the cell lysates.

Western Blot Analysis

The following antibodies were used: rabbit anti-ABCG1 (NB400-132, 1:500; Novus Biologicals); rabbit anti-ABCA1 (NB400-105, 1:500; Novus Biologicals); mouse anti-tubulin (clone KMX-1, catalog MAB3408, 1:500; Millipore); mouse anti-β-actin (A1978, 1:4,000; Santa Cruz Biotechnology); rabbit anti-PPARG (ab41928, 1:1,000; Abcam); rabbit anti-RAGE (GTX23611, 1:1,000; GeneTex); rabbit anti-apoA1 (ab20453, 1:1,000; Abcam); rabbit anti-p44/42 mitogen-activated protein kinase (MAPK) (Erk1/2) (9102, 1:1,000; Cell Signaling); and mouse anti-phospho-p44/42 MAPK (Erk1/2) (9106, 1:1,000; Cell Signaling). After incubation with the indicated secondary antibodies, protein signals were visualized with an enhanced chemiluminescence detection system (Thermo Scientific) using the Odyssey Fc Dual-Mode Imaging system (LI-COR) or IRDye 680RD goat anti-mouse (1:25,000) (LI-COR) and IRDye 800CW goat anti-rabbit (1:10,000; LI-COR), and protein signals were visualized using the Odyssey Infrared Imaging System Model 9120 (LI-COR).

Luciferase Reporter Assays

Human *ABCG1* promoter A region spanning −1,104 to +37 base pairs (upstream of exon 1) cDNA was generated following published methods by Uehara et al. (18) and cloned into pCR-script vector. Subsequently, this cDNA for human *ABCG1* promoter A region (−1,104/+37) was cloned into the pGL3-basic vector using restriction sites *Kpn*I and *Hin*dIII. Before transfection, HEK293T cells were grown to 50–80% confluence on 12-well plates in DMEM supplemented with 10% FBS + 1% penicillin-streptomycin. Cells were transiently transfected with 1 μg mouse *Ager* cDNA in pcDNA3 vector on day 1, and then on day 2, cells were transiently transfected with 1 μg pGL3 luciferase firefly vector (Promega) containing human *ABCG1* promoter A or human *ABCA1* promoter cDNA (gift from Antonio Castrillo, Instituto de Investigaciones Biomédicas "Alberto Sols"), and 1 ng pRL-TK vector *Renilla* (Promega) (to normalize transfections) using Lipofectamine 2000 (Invitrogen). Luciferase activities were measured using the Dual-Luciferase Reporter Assay System (Promega) and were divided by *Renilla* activity to obtain a normalized value (in relative luciferase units). *ABCG1* deletion mutants were prepared as described by Uehara et al. Site-directed mutations to PPAR response element (PPRE) 1 (sense) and PPRE2 (antisense) sites (single mutations and a double mutation) on the human *ABCG1* promoter were constructed using the QuikChange II XL Site-Directed Mutagenesis Kit (Agilent Technologies).

Bioinformatics

The −413 to −303 region of the *ABCG1* promoter was compared with the high-quality vertebrate subset of Transfac Professional version 2013.2 (19) using the Match program (20) set to minimize false-positive results. Binding sites of 19 unique transcription factors were found. Among these were binding sites for Pparg (V$PPARG_02) (21,22). There are two V$PPARG_02 sites, both of which were at −330, one in the sense direction and the other in the antisense direction. The most conserved regions of the site core sequence were used to design single–base pair substitutions to interfere with binding. In the following text, the core recognition element is capitalized and the replacement nucleotide is indicated in boldface. On the sense strand, the following substitutions were made:

S1: −325G→C
gagatGGGTAgattttcctactt
gagat**C**GGTAgattttcctactt

For antisense, the following substitutions were made:

A1: −313C→G
gagatgggtagatTTTCCtactt
gagatgggtagatTTTC**G**tactt

Electrophoretic Mobility Shift Assays

Nuclear protein extracts were prepared from THP-1 cells, and electrophoretic mobility shift assays (EMSAs) were performed using the Odyssey EMSA Buffer Kit (LI-COR) and 10X orange loading dye (LI-COR) according to the manufacturer's instructions. Gels were visualized using a LI-COR Odyssey imager. The *PPARG* DNA probe sequences used were as follows:

Sense strand: 5′-/5IRD700/GAGATGGGTAGATTTTCCTACTT-3′
Antisense strand: 5′-/5IRD700/CTCTACCCATCTAAAAGGATGAA-3′

HDL Cholesterol, Total Cholesterol, and Triglyceride Measurements

HDL cholesterol and total cholesterol concentrations were measured using colorimetric assays (Wako Diagnostics); triglyceride levels were measured enzymatically using a colorimetric assay (L-Type TG M Enzyme Color A; Wako Diagnostics).

Chromatin Immunoprecipitation

Chromatin immunoprecipitation (ChIP) assays were performed using the ChIP-IT Express enzymatic kit (Active Motif). ChIP-enriched DNA (2 μL) was used for quantitative real-time PCR for the *ABCG1* promoter using SYBR Green reagents and the following primers: forward primer, 5′-TTTGCCGTAATTGTTTTCAATG-3′; reverse primer, 5′-GCAGGGTTACTAAAGGGCAGT-3′.

Laser Capture Microdissection

Aortic arches from the indicated *Ldlr*$^{-/-}$ or *Ldlr*$^{-/-}$/*Ager*$^{-/-}$ mice were subjected to laser capture microdissection (LCM) of CD68-expressing cells (detected by rat anti-mouse CD68 clone FA-11 (MCA1957; AbD Serotec) using a Leica LMD6500 Laser Microdissection System and quantitative real-time PCR for measuring *Abca1*, *Abcg1*, and *Pparg* mRNA transcripts.

Oil Red O Staining

Oil red O staining of atherosclerotic lesions was performed according to the manufacturer's instructions (AMTS Inc.) (23).

Macrophage RCT

Male WT C57BL/6 or littermate *Ager*$^{-/-}$ mice were rendered diabetic with STZ for 2 months, and bone marrow was collected. BMDMs were prepared and radiolabeled with 5 μCi/mL ^{3}H-cholesterol and acetylated LDL (50 μg/mL) for 24 h. BMDMs were washed and injected into WT C57BL/6 nondiabetic mice. On the day of injection, recipient mice were housed individually with unlimited access to food and water. ^{3}H-cholesterol/acetylated LDL–loaded BMDMs (2.5–3.5 × 10^{6}/mL) were injected intraperitoneally. Blood was collected and plasma subjected to counting in a β-counter. Feces were collected continuously for 64 h. At 64 h, mice were humanely killed, and liver tissue was collected for further analyses. Results were expressed as a percentage of the counts per minute (cpm) injected as previously described (24).

Statistics

All data are reported as mean ± SEM unless otherwise stated (*n* is noted in figure legends). Data were analyzed with the Student *t* test or by ANOVA followed by two-tailed

distribution t test. $P \leq 0.05$ was considered statistically significant. Cholesterol efflux and RCT were log-transformed before analysis to ensure approximate normality and were analyzed in R. Experiments at each time point were analyzed separately to characterize the effect of each genotype/disease state combination on RCT at that time. Additionally, each genotype/disease state combination experiment was analyzed separately at different times to characterize the effect of time on RCT for that combination. Both the Fligner-Killeen test (25) and visual inspection showed heteroscedasticity, so the Welch test for the comparison of several means (26) was used instead of standard ANOVA to estimate significance. Significance of comparisons was estimated using the Westfall method (27,28) as implemented in multcomp (29), with heteroscedasticity accounted for by a Sandwich estimator (30) as implemented in Sandwich (31). The figures display means and SEs back-transformed to percentages. Supplementary Table 2 presents the Welch test P value, which is the probability that at least one of the conditions is not the same as the other. Supplementary Table 2 also gives the probability of ($Ager^{-/-}$ diabetic mice [DM] − $Ager^{-/-}$ nondiabetic mice [NDM]) − (WT DM − WT NDM), differing from 0 by chance (i.e., the probability that the effect of diabetes on RCT in $Ager^{-/-}$ mice differs from the effect of diabetes in WT mice). By simple algebraic manipulation, this expression is also equal to ($Ager^{-/-}$ DM – WT DM) – ($Ager^{-/-}$ NDM − WT NDM), which is the effect of deletion of *Ager* in diabetic mice relative to the effect on nondiabetic mice. This later expression shows whether the comparison of the effect of deletion of *Ager* in diabetic mice differs from the corresponding effect in nondiabetic mice.

RESULTS

RAGE Impairs Macrophage Cholesterol Efflux to ApoA1 and HDL in Diabetes

Primary BMDMs were retrieved from WT male C57BL/6 mice after 2 months of hyperglycemia induced by STZ. Controls were age- and sex-matched nondiabetic mice treated with intraperitoneal injections of the vehicle for STZ citrate buffer. BMDMs were cultured in concentrations of glucose consistent with the glycemic state of the mice from which they were retrieved. WT BMDMs retrieved from diabetic animals displayed significantly reduced cholesterol efflux to apoA1 and HDL versus BMDMs from nondiabetic WT mice ($P < 0.01$ and $P < 0.001$, respectively) (Fig. 1*A* and *B* and Supplementary Table 2). In the nondiabetic state, although deletion of *Ager* imparted no significant effect on cholesterol efflux to apoA1 versus WT BMDMs, significantly higher cholesterol efflux to HDL was observed ($P < 0.0001$) (Fig. 1*A* and *B* and Supplementary Table 2). In the diabetic state, deletion of *Ager* resulted in significantly higher cholesterol efflux to both apoA1 and HDL compared with WT BMDMs ($P < 0.001$) (Fig. 1*A* and *B* and Supplementary Table 2).

Because it has been reported that mRNA transcript and protein levels of *Abca1* and *Abcg1*, principal regulators of cholesterol efflux to apoA1 and HDL, respectively, are reduced in murine and human diabetes (9,10,32,33), we tested the role of RAGE. The mRNA transcript and protein levels of *Abca1* were lower after 2 months of hyperglycemia in WT BMDMs (Fig. 1*C* and *D*). In the nondiabetic state, *Abca1* mRNA transcript levels did not differ significantly between WT and $Ager^{-/-}$ BMDMs, but ABCA1 protein levels were significantly higher in $Ager^{-/-}$ versus WT BMDMs. In the diabetic state, higher levels of *Abca1* mRNA transcripts and protein were observed between $Ager^{-/-}$ and WT BMDMs (Fig. 1*C* and *D*).

Diabetes resulted in a significant reduction in *Abcg1* mRNA transcripts and ABCG1 protein in WT BMDMs versus the nondiabetic state (Fig. 1*E* and *F*). In both nondiabetic and diabetic BMDMs, deletion of *Ager* resulted in significantly higher levels of *Abcg1* mRNA transcripts and ABCG1 protein than in WT BMDMs (Fig. 1*E*). These data indicate that diabetes exerted significant effects on the downregulation of ABCA1 and ABCG1 transporters through RAGE.

To directly test the effects of glucose, we incubated nondiabetic mice BMDMs from WT mice in high glucose (25 mmol/L) for 7 days versus normal glucose levels (5.5 mmol/L) and determined *Abca1* and *Abcg1* mRNA levels. No significant differences were observed in mRNA levels in nondiabetic WT BMDMs cultured for 7 days in 5.5 or 25 mmol/L D-glucose (Supplementary Fig. 1*A* and *B*).

Additionally, we retrieved primary peritoneal macrophages (without thioglycollate treatment) and prepared mRNA immediately upon retrieval. Compared with WT peritoneal macrophages from nondiabetic mice, WT diabetic peritoneal macrophages displayed significantly lower levels of *Abca1* and *Abcg1* mRNA transcripts. In the nondiabetic state, a significant increase in *Abcg1* mRNA transcripts was observed in $Ager^{-/-}$ versus WT peritoneal macrophages, and in the diabetic state, $Ager^{-/-}$ peritoneal macrophages displayed significantly higher levels of both *Abca1* and *Abcg1* mRNA transcripts (Supplementary Fig. 1*C* and *D*). These results are completely analogous to those observed in primary murine BMDMs (Fig. 1*C* and *E*).

AGE-RAGE Interaction Suppresses Cholesterol Efflux to ApoA1 and HDL in Human THP-1 Cells

To ensure that the results applied to cells that normally express RAGE and are of human origin, we treated THP-1 cells with carboxymethyllysine (CML)-AGE, which was previously shown to be a specific AGE ligand of RAGE that accumulates in human atherosclerotic lesions (34). Compared with vehicle/scramble siRNA treatment, CML-AGE resulted in significantly reduced cholesterol efflux to apoA1 and HDL ($P < 0.0001$) (Fig. 2*A* and *B*). RNA interference (RNAi) knockdown of *AGER* in CML-AGE–treated THP-1 cells resulted in significantly higher cholesterol efflux to apoA1 ($P < 0.01$) and HDL ($P < 0.0001$)

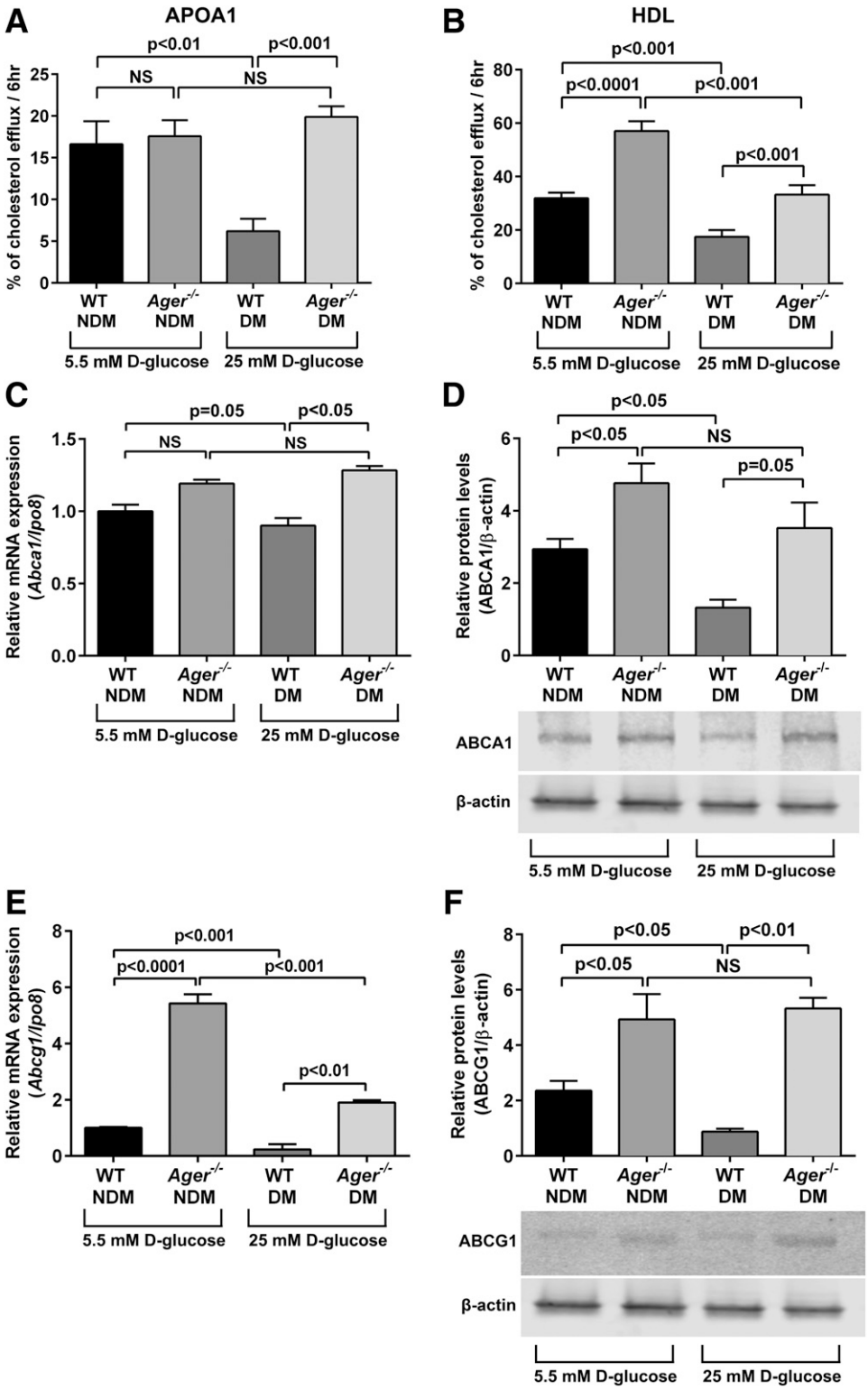

Figure 1—Effect of diabetes on cholesterol efflux to apoA1 or HDL and regulation of cholesterol transporters by *Ager* in primary murine BMDMs. Primary BMDMs were retrieved from nondiabetic and diabetic WT (2 months of hyperglycemia) and *Ager*$^{-/-}$ mice and were cultured in concentrations of glucose consistent with the glycemic state of the mice from which they were retrieved. BMDMs were labeled with ^{3}H-cholesterol and treated with acetylated LDL and fatty acid–free BSA (1%) for 24 h. *A* and *B*: To mediate cholesterol efflux, cells were treated with apoA1 (5 μg/mL) (*A*) or HDL (100 μg/mL) (*B*) for 6 h, and supernatant was collected. Percent cholesterol efflux is the radioactivity in the supernatant divided by the sum of the radioactivity measured in the supernatant and the cell lysates from $n \geq 5$ mice/group. *C* and *D*: BMDMs were retrieved from WT or *Ager*$^{-/-}$ mice and subjected to quantitative real-time PCR for detection of *Abca1* mRNA transcript (*C*) and ABCA1 protein (*D*) analysis ($n = 3$ mice/group). *E* and *F*: BMDMs were prepared as in *C* and *D* and assessed for levels of *Abcg1* mRNA transcripts (*E*) and ABCG1 protein (*F*) ($n = 3$ mice/group). Error bars represent mean ± SEM. hr, hour; NS, not statistically significant.

compared with scramble siRNA/CML treatment (Fig. 2*A* and *B*).

Treatment of THP-1 cells with CML-AGE in the presence of scramble siRNA resulted in significant suppression of *ABCA1* and *ABCG1* mRNA transcripts ($P < 0.01$) (Fig. 2*C* and *D*). RNAi knockdown of *AGER* resulted in significantly higher levels of *ABCA1* and *ABCG1* mRNA transcripts versus scramble siRNA/CML-AGE treatment ($P < 0.001$ and $P < 0.01$, respectively) (Fig. 2*C* and *D*).

At the protein level, Western blotting revealed a trend to lower levels of ABCA1 protein in CML-AGE–treated THP-1 cells; in the presence of RNAi knockdown of *AGER*, ABCA1 protein levels were similar to those in non-CML-AGE–treated cells (Fig. 2*E*). In the case of

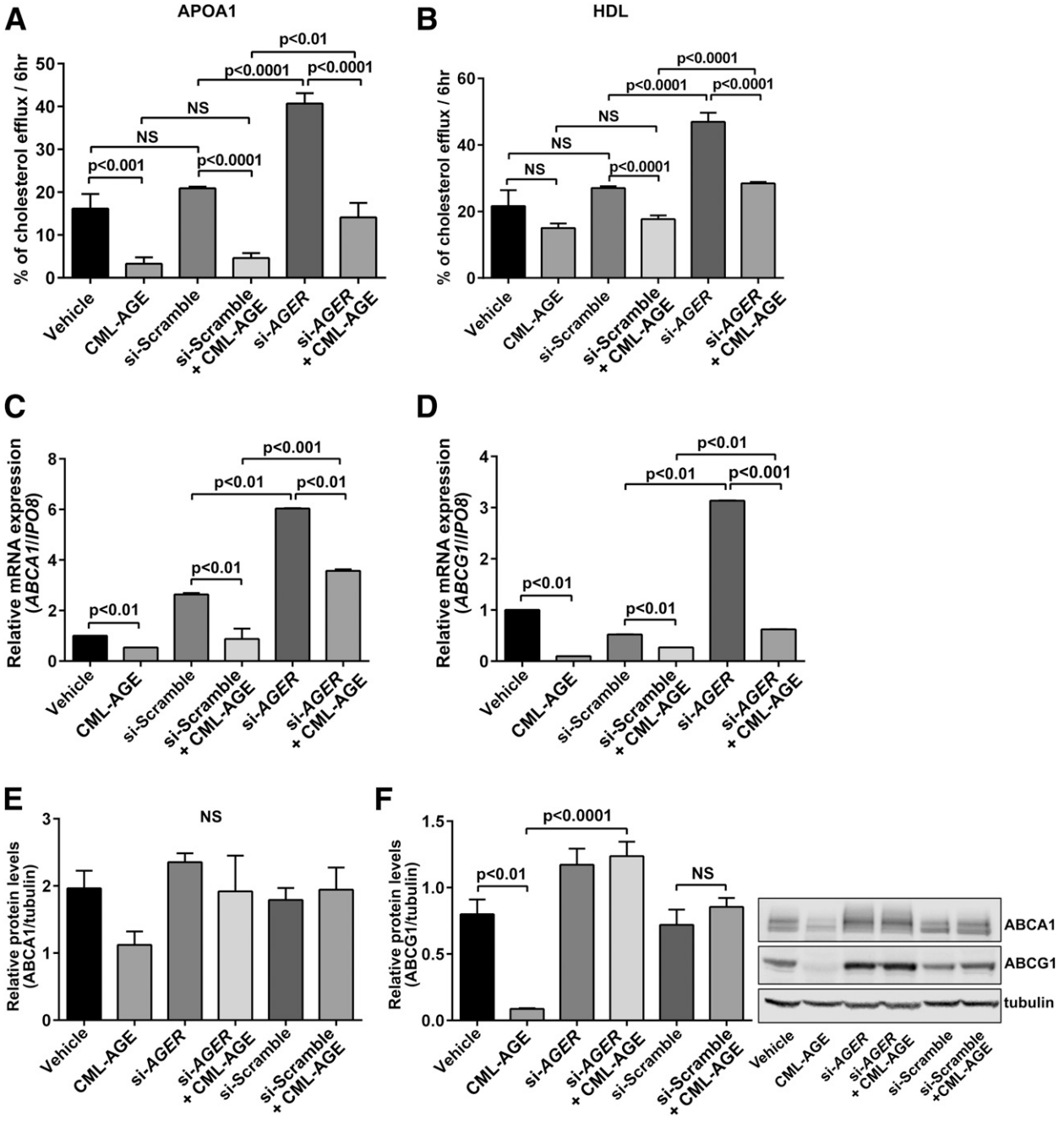

Figure 2—CML-AGE suppresses cholesterol efflux and regulation of *ABCA1* and *ABCG1* in human THP-1 cells: effects of *AGER*. Human THP-1 cells were transfected with siRNA-scramble or siRNA-*AGER* and treated with vehicle (PBS) or CML-AGE (10 μg/mL) for 16 h. *A* and *B*: Cholesterol efflux was measured to apoA1 (25 μg/mL) (*A*) or HDL (100 μg/mL) (*B*) for 6 h, and supernatant was collected. Percent cholesterol efflux is the radioactivity in the supernatant divided by the sum of the radioactivity measured in the supernatant and the cell lysates ($n = 5$ independent experiments). *C* and *D*: mRNA transcripts were determined for *ABCA1* (*C*) and *ABCG1* (*D*) by quantitative real-time PCR ($n = 3$ independent experiments). *E* and *F*: Protein expression levels by Western blotting were determined for ABCA1 (*E*) and ABCG1 (*F*) ($n = 3$ independent experiments). Error bars represent mean ± SEM. NS, not statistically significant.

ABCG1, treatment with CML-AGE resulted in a significant suppression of ABCG1 protein levels versus vehicle ($P < 0.01$) (Fig. 2*F*). RNAi knockdown of *AGER* in the presence of CML-AGE resulted in significantly higher levels of ABCG1 protein compared with CML-AGE treatment ($P < 0.0001$) (Fig. 2*F*). Thus, in human RAGE-expressing THP-1 cells, RAGE ligand CML-AGE reduces cholesterol efflux to apoA1 and HDL at least in part through regulation of ABCA1 and ABCG1.

RAGE Mediates Impaired RCT in Diabetic Macrophages

Based on in vitro findings that RAGE contributes to suppression of macrophage cholesterol efflux to apoA1 and HDL, particularly in diabetes, we tested the effects of RAGE on macrophage RCT in vivo. WT and *Ager*$^{-/-}$ mice were rendered hyperglycemic with STZ or treated with the control citrate buffer (nondiabetes) for 2 months. BMDMs were isolated, loaded with radiolabeled cholesterol, and injected into WT nondiabetic mice. As shown in Fig. 3*A* and *B*, in WT mice, diabetes resulted in reduced macrophage RCT to plasma at 43 and 64 h postinjection of WT BMDMs ($P < 0.001$, and $P < 0.01$, respectively). In nondiabetic BMDMs, no statistically significant effects of *Ager* deletion were noted at 43 or 64 h postinjection (Fig. 3*A* and *B*). In diabetic BMDMs, however, deletion of *Ager* resulted in significantly higher RCT to plasma at 43 and 64 h postinjection ($P < 0.001$ and $P < 0.01$, respectively) (Fig. 3*A* and *B* and Supplementary Table 2).

Diabetes resulted in a trend to reduced macrophage RCT to the liver versus the nondiabetic state (Fig. 3*C* and Supplementary Table 2). Although deletion of *Ager* had no significant effect on macrophage RCT to the liver in the nondiabetic state, significantly higher RCT in diabetic BMDMs devoid of *Ager* was noted compared with diabetic WT BMDMs ($P < 0.01$) (Fig. 3*C* and Supplementary Table 2). In feces of WT mice, diabetes resulted in significantly reduced macrophage RCT ($P < 0.01$). Although deletion of *Ager* in nondiabetic BMDMs resulted in modest but significantly lower RCT to feces versus WT nondiabetic BMDMs, trends to higher RCT to feces were observed in diabetic BMDMs devoid of *Ager* compared with diabetic WT BMDMs (Fig. 3*D* and Supplementary Table 2).

We measured plasma levels of HDL and found that diabetes resulted in significantly lower levels of HDL in WT mice than in age-matched WT nondiabetic mice (35.1 ± 0.8 vs. 41.7 ± 2.3, $P < 0.01$) (Fig. 3*E*). In the nondiabetic state, levels of HDL did not differ by *Ager* genotype (41.7 ± 2.3 vs. 42.3 ± 1.4 in WT nondiabetic vs. *Ager*$^{-/-}$ nondiabetic mice,

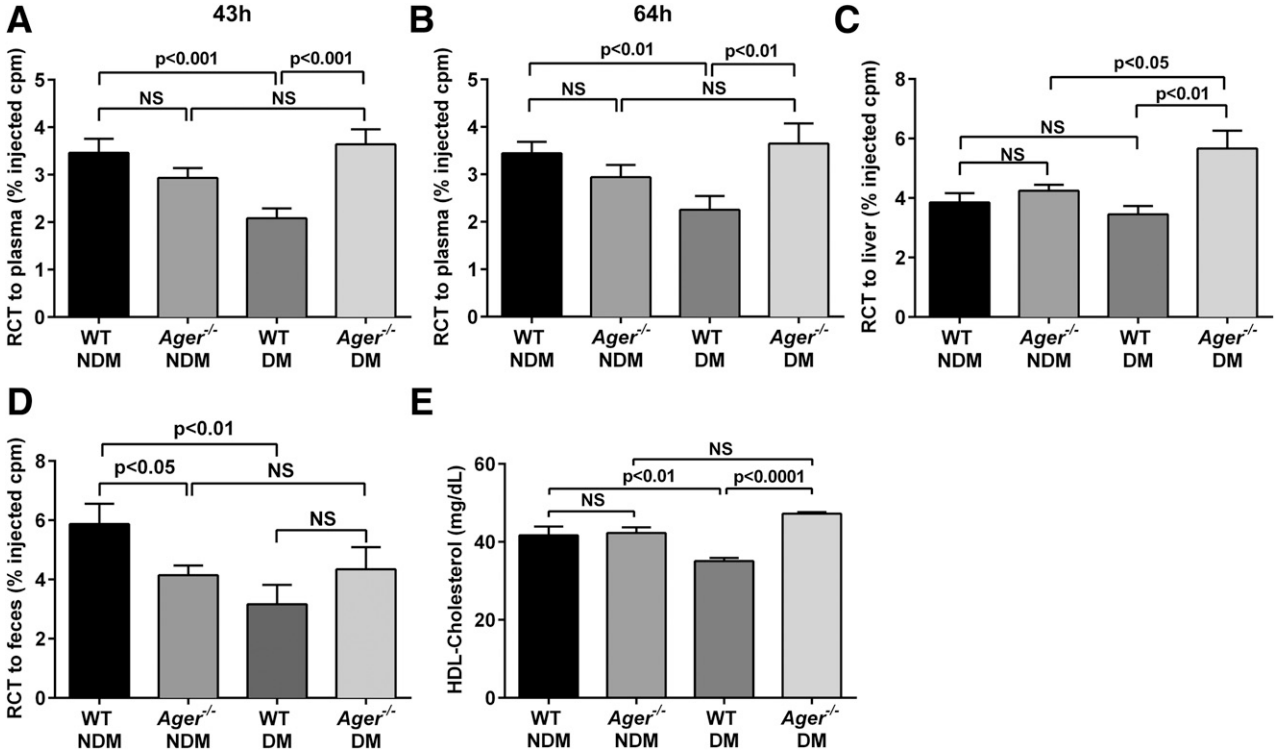

Figure 3—Macrophage RCT and plasma HDL levels: effects of *Ager*. WT nondiabetic mice were injected subcutaneously with ^{3}H-cholesterol–labeled, acetylated LDL–loaded BMDMs from nondiabetic or diabetic (at least 2 months hyperglycemia) WT or *Ager*$^{-/-}$ mice. Plasma distribution of ^{3}H-cholesterol was measured at 43 h (*A*) and 64 h (*B*). Hepatic ^{3}H-cholesterol tracer levels were measured after 64 h (*C*), and feces were collected continuously from 0 to 64 h after injection (*D*). Data are percentage of the ^{3}H-cholesterol tracer relative to that of total cpm tracer injected ± SEM. $n \geq 6$ mice/group. *E*: Plasma HDL cholesterol levels were measured in nondiabetic and diabetic WT and *Ager*$^{-/-}$ mice ($n = 10$ mice/group). Error bars represent mean ± SEM. NS, not statistically significant.

respectively; *P* not significant) (Fig. 3*E*). In contrast, diabetic *Ager*$^{-/-}$ mice displayed significantly higher levels of HDL versus age-matched WT diabetic mice (47.2 ± 0.4 vs. 35.1 ± 0.8, $P < 0.0001$) (Fig. 3*E*). Levels of total cholesterol were tested (Supplementary Table 3). In the nondiabetic state, no significant effects of *Ager* genotype were seen. Total levels of cholesterol were higher in diabetic versus nondiabetic WT mice (120.7 ± 4.0 vs. 96.4 ± 3.2, $P < 0.001$). Diabetic *Ager*$^{-/-}$ mice displayed significantly lower levels of total cholesterol than their diabetic WT counterparts (95.4 ± 2.9 vs. 120.7 ± 4.0, $P < 0.001$) (Supplementary Table 3).

On the basis of these findings of higher levels of plasma HDL in diabetic mice devoid of *Ager*, we tested mRNA transcript and protein levels of *Apoa1* and *Abca1* in mouse liver tissue because apoA1 and ABCA1 are critical for HDL production (35). *Ager* genotype had no effect on mRNA transcript levels of *Apoa1* (Supplementary Fig. 2*A*) or *Abca1* (Supplementary Fig. 2*B*) in nondiabetic mice. However, diabetes resulted in a significant reduction in *Apoa1* and *Abca1* mRNA transcripts versus the nondiabetic state in WT mice ($P < 0.05$). Levels of *Apoa1* and *Abca1* mRNA transcripts were lower in diabetic *Ager*$^{-/-}$ versus diabetic WT liver tissue ($P < 0.001$ and $P < 0.05$,

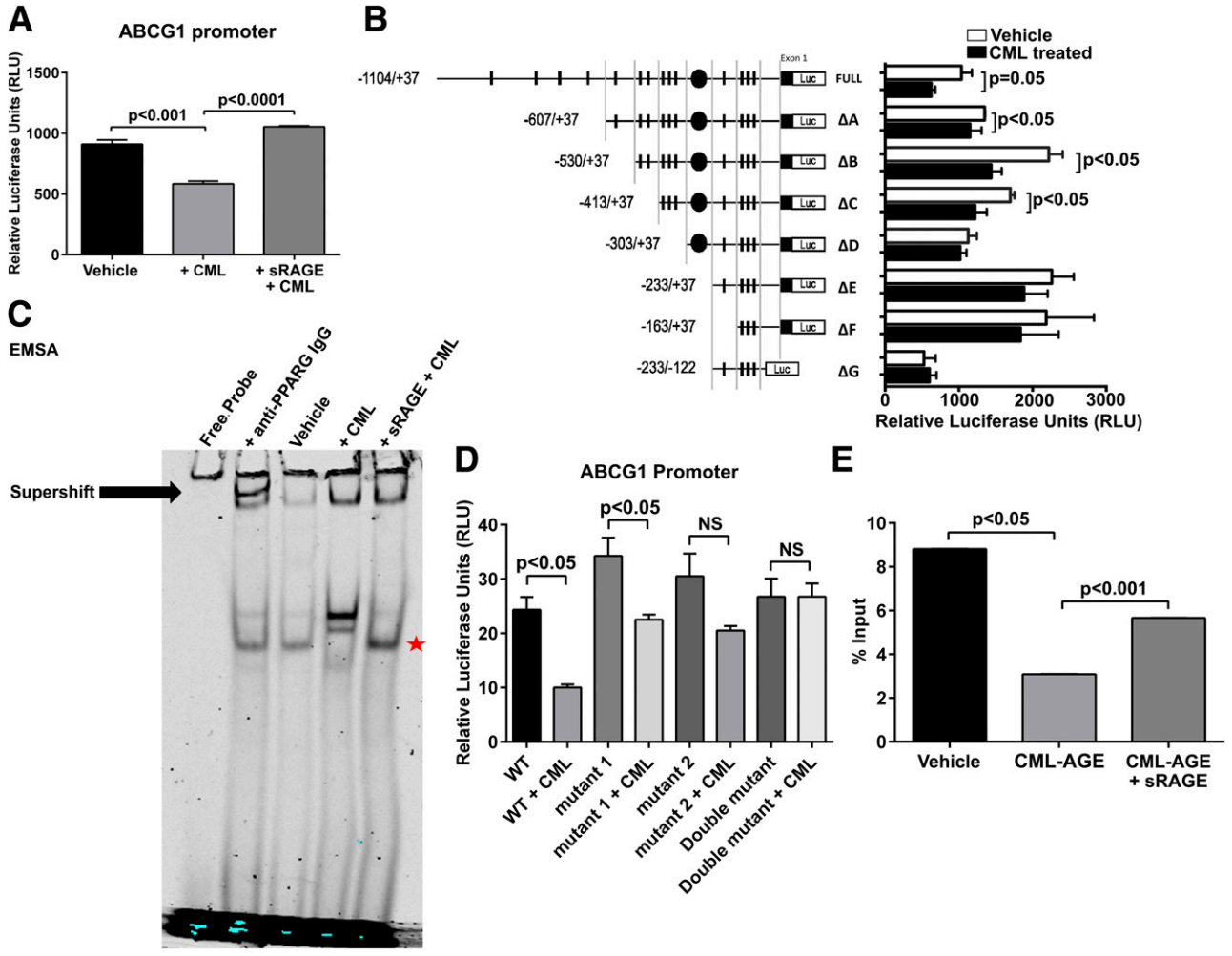

Figure 4—Molecular characterization of CML-AGE modulation on the human *ABCG1* promoter. Luciferase activities were measured in RAGE-expressing HEK293T cells transfected with 1 μg promoter reporter plasmid (pGL3) and 1 ng pRL-TK-*Renilla*. Firefly luciferase activity was divided by *Renilla* activity to obtain a normalized value as an RLU. Results are mean ± SEM. *A*: Activity of human *ABCG1* promoter treated with CML-AGE (300 μg/mL) or CML-AGE (300 μg/mL) and sRAGE (6,000 μg/mL) (n = 3 independent experiments). *B*: Activity of human *ABCG1* promoter deletion mutants treated with vehicle (PBS) or CML-AGE (300 μg/mL) for 16 h (n = 6 independent experiments). *C*: EMSA of nuclear protein extracts (THP-1 cells) (5 μg) treated with anti-PPARG IgG (4 μg) (supershift); vehicle (PBS); CML-AGE (10 μg/mL); and CML-AGE (10 μg/mL) + sRAGE (200 μg/mL). CML-AGE reduces nuclear protein binding to the *ABCG1* promoter containing PPARG elements, which is prevented by sRAGE treatment. Data are representative of three independent EMSAs. The star represents rescue of band with sRAGE treatment. *D*: Activity of human *ABCG1* promoter containing site-directed mutations at the PPRE sites treated with vehicle (PBS) or CML-AGE (300 μg/mL) (n = 4 independent experiments). *E*: ChIP analysis of the ABCG1 promoter region to PPARG in human THP-1 cells treated with vehicle (PBS), CML-AGE (10 μg/mL), or CML-AGE + sRAGE (200 μg/mL) for 16 h (n = 3 independent experiments). Quantitative real-time PCR analysis of ABCG1 promoter region using primers containing both PPRE1 and PPRE2 was determined. Error bars represent mean ± SEM. NS, not statistically significant.

respectively) (Supplementary Fig. 2*A* and *B*). Deletion of *Ager* resulted in increased apoA1 protein levels in nondiabetic mouse livers ($P < 0.01$), with trends to increased protein levels of apoA1 in diabetic mouse liver devoid of *Ager* versus WT (Supplementary Fig. 2*C*). No difference was observed in ABCA1 protein levels between nondiabetic $Ager^{-/-}$ and WT liver tissue, whereas protein levels were significantly higher in diabetic $Ager^{-/-}$ liver than in diabetic WT ($P < 0.05$) and nondiabetic $Ager^{-/-}$ ($P < 0.05$) livers (Supplementary Fig. 2*D*). These findings suggest that the higher levels of HDL in mice devoid of *Ager*, particularly in the diabetic state, are likely accounted for by significantly higher levels of ABCA1 protein in the liver.

AGE-RAGE Interaction and Molecular Regulation of ABCG1

To define the molecular mechanisms accounting for these findings, human *ABCA1* and *ABCG1* promoter reporter luciferase constructs were transfected into *AGER*-transfected HEK293T cells (HEK293T cells do not natively express RAGE); treatment of these cells with CML-AGE resulted in significant suppression of both *ABCA1* ($P < 0.05$) (Supplementary Fig. 3*A*) and *ABCG1* ($P < 0.001$) (Fig. 4*A*) promoter luciferase activity. We focused on the effects of RAGE on molecular regulation of *ABCG1* because the greatest reduction in transcription of the two transporters by CML-AGE/RAGE in macrophages was on *ABCG1* and because macrophage cholesterol efflux to HDL was most potently affected by RAGE. Supporting the RAGE dependence of these findings on CML-AGE–mediated suppression of *ABCG1* promoter luciferase activity in the absence of *AGER* transfection in HEK293T cells, CML-AGE exerted no suppressive effects on *ABCG1* promoter luciferase activity (Supplementary Fig. 3*B*). Furthermore, the effect of CML-AGE treatment on suppression of the *ABCG1* promoter luciferase activity in *AGER*-expressing HEK293T cells was prevented by incubation with sRAGE, the extracellular ligand-binding domain of RAGE ($P < 0.0001$) (Fig. 4*A*).

A series of deletion mutants of the human *ABCG1* promoter (1,104/+37) was prepared as described by Uehara et al. (18). CML-AGE treatment resulted in significant suppression of promoter luciferase activity in full-length and deletion mutants A, B, and C (Fig. 4*B*). However, in deletion mutants D, E, F, and G, there were no suppressive effects of CML-AGE, thereby implicating elements within C but not D in the suppressive effects of CML-AGE on promoter reporter luciferase activity. As shown in Supplementary Table 4, multiple putative transcription factor binding sites within −413 to −304 were identified. Of note, NRLH3 (liver X receptor [LXR]-α) putative binding sites were not identified within this region (36). Consistent with this finding, diabetes exerted no significant effect on mRNA transcript levels of *Nr1h3* (Lxr-α) or *Nrlh2* (Lxr-β) compared with nondiabetic BMDMs (Supplementary Fig. 4*A* and *B*). Additionally, CML-AGE exerted no suppressive effect on LXR agonist T0901317–mediated increase in *ABCA1* (Supplementary Fig. 5*A*) or *ABCG1* (Supplementary Fig. 5*B*) promoter reporter luciferase activity, suggesting a mechanism of action independent of LXRs.

Given the known potent effects of PPARG on macrophage properties (37–39), we determined whether putative PPREs within the human *ABCG1* promoter were linked to the suppressive effects of CML-AGE. Although LXR putative binding sites were not observed in the region of interest (−413 to −304) within the *ABCG1* promoter, we identified at least two putative PPREs in this region. First, to directly assess the binding of RAGE-expressing THP-1 cell nuclear extract to the PPRE1- and PPRE2-containing binding elements on the −413 to −304 promoter region, we performed EMSAs using a consensus probe incorporating both PPRE sites. As shown in Fig. 4*C*, CML-AGE reduced nuclear protein binding to the *ABCG1* promoter elements containing the two indicated PPREs in a manner prevented by sRAGE. Of note, the supershift experiments demonstrated the specific bands of interest by virtue of shifting (reduced intensity) in the presence of anti-PPARG IgG (Fig. 4*C*).

Second, we performed site-directed mutagenesis of PPRE sense (gagatGGGTAgattttcctactt) and PPRE antisense (gagatgggtagatTTTCCtactt) and tested promoter reporter luciferase activity in CML-AGE versus vehicle-treated RAGE-expressing HEK293T cells. As shown in Fig. 4*D*, mutation of PPRE antisense (mutation 2) and both PPRE antisense and PPRE sense (mutation 2 and 1) prevented the suppressive effects of CML-AGE on the promoter reporter luciferase activity in the −413 to −304 region. Taken together, these results demonstrate that CML-AGE suppresses *ABCG1* promoter activity in a manner that can be prevented by sRAGE and that CML-AGE mediates suppressive effects on the −413 to −304 region on the *ABCG1* promoter in a manner involving the antisense (TTTCC) core motif recognized by PPARG.

Finally, we performed ChIP assays to directly study the effects of CML-AGE on PPARG transcription factor recruitment to the −413 to −304 *ABCG1* promoter region. A robust signal of *ABCG1* mRNA transcription by quantitative real-time PCR was noted in THP-1 under basal conditions; when THP-1 cells were treated with CML-AGE, this signal was significantly reduced by >50% ($P < 0.05$) (Fig. 4*E*). Treatment with sRAGE significantly rescued the suppressive effects of CML-AGE on *ABCG1* mRNA transcription levels in the ChIP assay ($P < 0.001$) (Fig. 4*E*). Thus, CML-AGE suppresses PPARG recruitment to the ABCG1 promoter locus in the promoter region −413 to −304 in a RAGE-dependent manner. Consistent with the principal effects of CML-AGE/RAGE on PPARG-dependent mechanisms, treatment of CML-AGE–treated THP-1 cells with the PPARG agonist rosiglitazone (10 μmol/L) partially, but significantly, rescued the CML-AGE–mediated suppressive effects on *ABCG1* mRNA transcripts ($P < 0.01$) (Supplementary Fig. 5*C*).

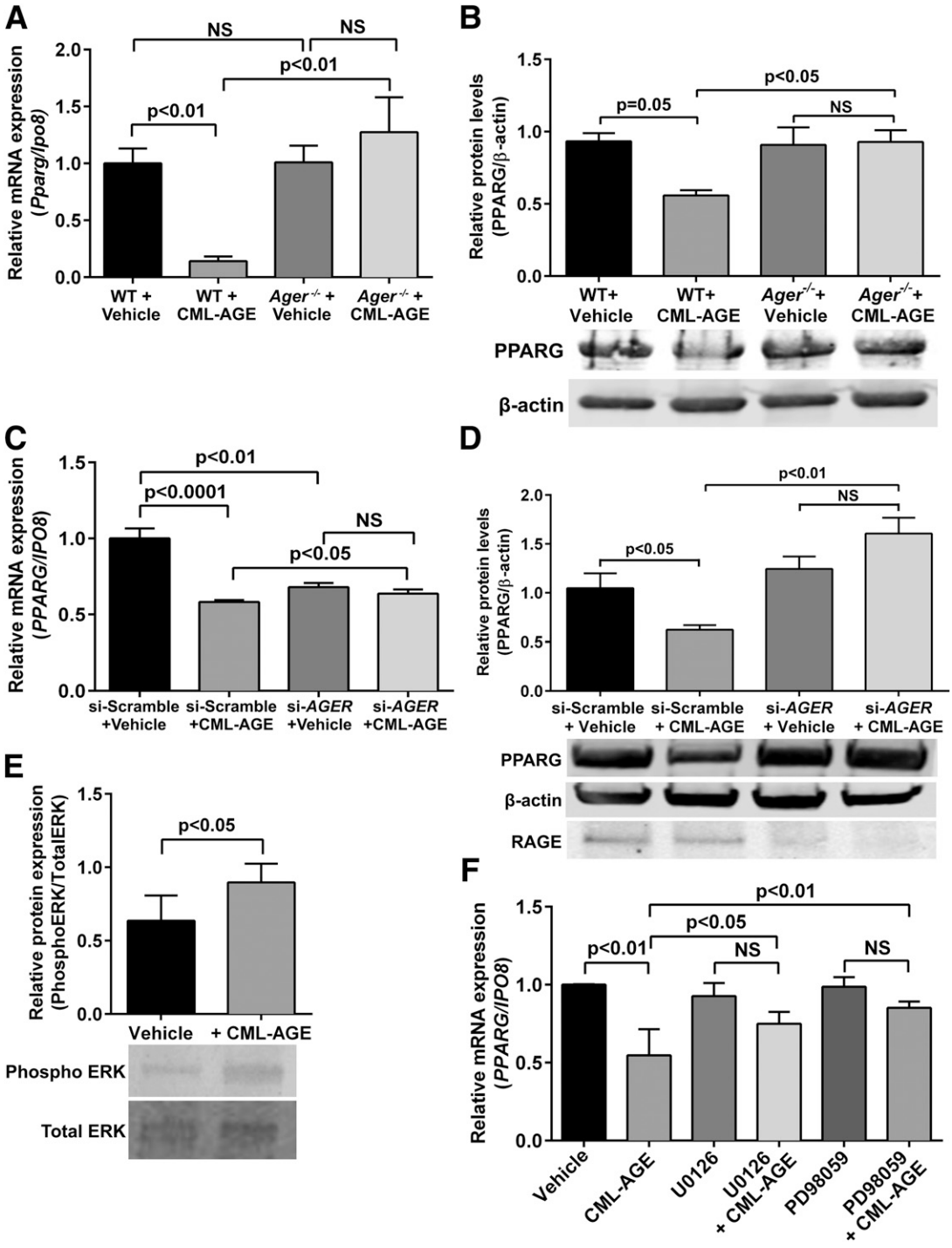

Figure 5—CML-AGE modulates PPARG levels: effect of RAGE. mRNA transcript (*A*) and Western blot (*B*) analysis of PPARG in primary BMDMs retrieved from diabetic WT and *Ager*$^{-/-}$ mice treated with vehicle (PBS) or CML-AGE (10 μg/mL) for 16 h (n = 3 mice/group). mRNA transcript (*C*) and Western blot (*D*) analysis of PPARG and RAGE in human THP-1 cells transfected with siRNA-scramble or siRNA-*AGER* and treated with vehicle (PBS) or CML-AGE (10 μg/mL) for 16 h (n = 3 independent experiments). *E*: Western blot analysis of phospho ERK and total ERK in human THP-1 cells after treatment with CML-AGE (10 μg/mL) for 16 h (n = 3 independent experiments). *F*: Human THP-1 cells were treated with vehicle or CML-AGE (10 μg/mL) with or without the ERK1/2 inhibitor (20 μmol/L U0126 or 75 μmol/L PD98059) for 30 min before treatment with vehicle or CML-AGE (10 μg/mL) for 16 h. mRNA transcript levels for *PPARG* were determined (n = 4 independent experiments). Error bars represent mean ± SEM. NS, not statistically significant.

CML-AGE/RAGE and Modulation of Levels of PPARG in BMDMs and RAGE-Expressing THP-1 Cells

These findings prompted us to test whether CML-AGE affected levels of PPARG. First, WT BMDMs treated with CML-AGE displayed a reduction in *Pparg* mRNA (Fig. 5*A*) and PPARG protein (Fig. 5*B*) compared with vehicle-treated WT cells ($P < 0.01$ and $P = 0.05$, respectively). In contrast, when *Ager*$^{-/-}$ BMDMs were treated with CML-AGE, no reduction in *Pparg* mRNA or PPARG protein levels was noted (Fig. 5*A* and *B*). Similarly, in CML-AGE–treated THP-1 cells, treatment with siRNA-*AGER* versus siRNA-scramble prevented the effects of CML-AGE on reducing levels of *PPARG* mRNA and PPARG protein ($P < 0.05$ and $P < 0.01$, respectively) (Fig. 5*C* and *D*).

To examine the molecular mechanisms by which CML-AGE suppresses PPARG binding to the *ABCG1* promoter, we assessed the MAPK pathway because it has been previously demonstrated to be an important regulator of PPARG expression (40). Treatment of THP-1 cells with CML-AGE resulted in increased phospho/total ERK versus treatment with vehicle ($P < 0.05$) (Fig. 5*E*). Pretreatment of THP-1 cells with the selective MAPK inhibitor U0126 or PD98059 prevented the effects of CML-AGE on suppression of *PPARG* mRNA versus vehicle (Fig. 5*F*). Thus, the molecular mechanism by which CML-AGE suppresses PPARG is at least partly through the MAPK pathway.

Rescue of CML-AGE Modulation on THP-1 Cell Cholesterol Efflux and Expression of ABCG1 and Modulation of *Pparg* mRNA in Atherosclerotic Plaques in Diabetic *LDLr*$^{-/-}$ Mice

To definitively link the suppressive effects of CML-AGE on cholesterol efflux to HDL to regulation of *ABCG1,* we overexpressed human *ABCG1* in THP-1 cells and treated the cells with CML-AGE versus vehicle. CML-AGE treatment resulted in reduced cholesterol efflux to HDL ($P < 0.01$) (Fig. 6*A*), which was prevented by *ABCG1* overexpression compared with CML-AGE treatment alone ($P < 0.0001$) (Fig. 6*A*). To unequivocally link PPARG reduction to the suppression of *ABCG1* transcription, we overexpressed human *PPARG* in THP-1 cells to determine whether this rescued the suppressive effects of CML-AGE on *ABCG1* and *ABCA1* mRNA transcript levels. Although CML-AGE resulted in reduced *ABCG1* and *ABCA1* mRNA transcripts versus vehicle in THP-1 cells ($P < 0.001$ and $P < 0.0001$, respectively) (Fig. 6*B* and *C*), transient transfection with *PPARG* cDNA prevented the suppressive effects of CML-AGE because levels of *ABCG1* were about fivefold higher

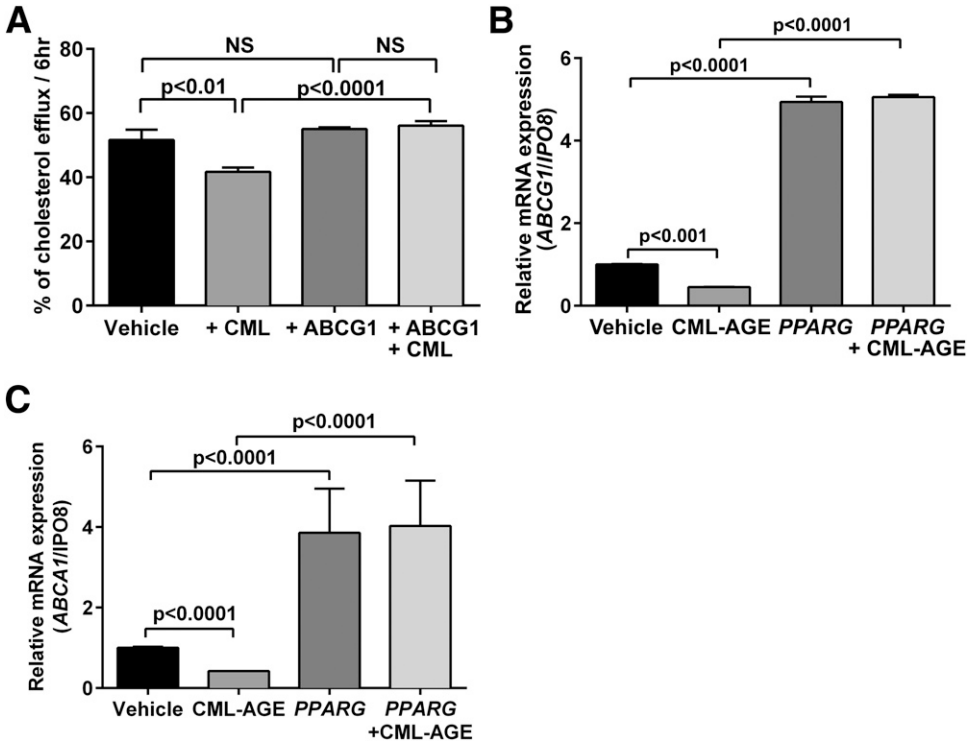

Figure 6—Effects of PPARG on CML-AGE–mediated downregulation of *ABCA1* and *ABCG1*. *A*: Human THP-1 cells were transfected with human *ABCG1* cDNA and treated with vehicle (PBS) or CML-AGE (10 μg/mL) for 16 h. Cholesterol efflux was measured to HDL (100 μg/mL) for 6 h, and supernatant was collected. Percent cholesterol efflux is the radioactivity in the supernatant divided by the sum of the radioactivity measured in the supernatant and the cell lysates ($n = 3$ independent experiments). *B* and *C*: Human THP-1 cells were transfected with human *PPARG* cDNA and treated with vehicle (PBS) or CML-AGE (10 μg/mL) for 16 h. mRNA transcript levels were determined for *ABCG1* (*B*) or *ABCA1* (*C*) ($n = 3$ independent experiments). Error bars represent mean ± SEM. NS, not statistically significant.

and levels of *ABCA1* were about fourfold higher in *PPARG*-overexpressed cells versus CML-AGE treatment alone ($P < 0.0001$ in each case) (Fig. 6*B* and *C*).

Next, to test whether deletion of *Ager* modulates lesional macrophage levels of *Abca1*, *Abcg1*, and *Pparg* in diabetic atherosclerosis (12), mice devoid of *Ldlr*, either expressing or devoid of *Ager*, were rendered diabetic with STZ. Mice were fed a Western diet for 15 weeks, which has been shown to induce insulin resistance (41). The accumulation of fats, lipids, and CD68-expressing macrophages was significantly reduced in atherosclerotic plaques from diabetic $Ldlr^{-/-}$ mice devoid of *Ager* versus $Ldlr^{-/-}$ mice expressing *Ager* (Fig. 7*A*). LCM CD68-expressing macrophages from the aortic plaques of diabetic $Ldlr^{-/-}$ mice devoid of *Ager* displayed higher levels of *Abca1* mRNA transcripts ($P = 0.05$) and significantly higher levels of *Abcg1* and *Pparg* mRNA transcripts than macrophages retrieved from atherosclerotic plaques of diabetic *Ager*-expressing $Ldlr^{-/-}$ mice ($P < 0.05$) (Fig. 7*B*). The beneficial effects of *Ager* deletion were independent of the levels of glucose, total cholesterol, or total triglycerides; levels of plasma HDL were higher in $Ldlr^{-/-}$ mice than in *Ager*-expressing mice devoid of *Ldlr* ($P < 0.05$) (Table 1).

Finally, to complement the findings in type 1 diabetes, we performed additional experiments to test the role for RAGE in the regulation of *Abca1*, *Abcg1*, and *Pparg* in BMDMs from mice fed an HFD versus an LFD for 3 months. Compared with LFD, HFD feeding in WT mice resulted in significant suppression of *Abca1* and significant, but modestly higher levels of *Abcg1* and *Pparg* mRNA transcripts (Supplementary Fig. 7*A*–*C*). In BMDMs of HFD-fed $Ager^{-/-}$ mice, mRNA transcript levels of *Abca1*, *Abcg1*,

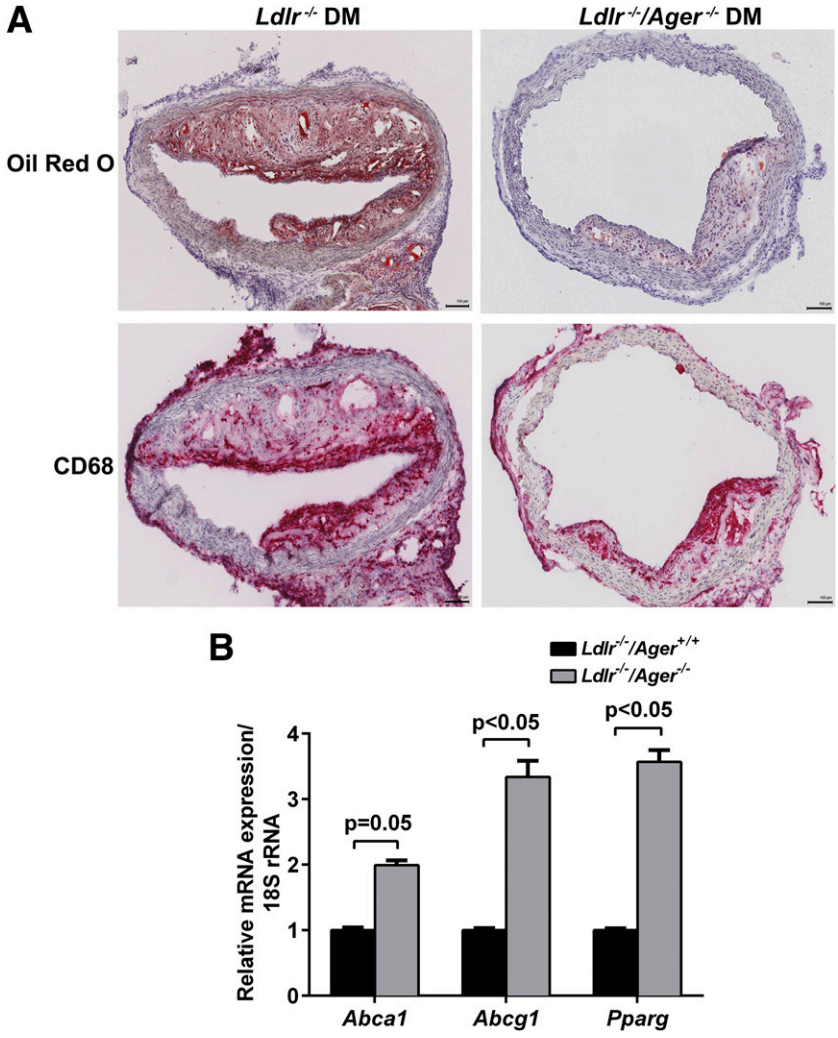

Figure 7—LCM of diabetic atherosclerotic aortic plaques: effects of *Ager*. Diabetic $Ldlr^{-/-}$ mice either expressing or devoid of *Ager* were fed a Western diet for 15 weeks; mice were killed at age 22 weeks. *A*: Aortic plaques were stained with anti-CD68 IgG (macrophages) and Oil red O (fats and lipids). Scale bar = 100 μm. Note that Supplementary Fig. 6 displays the much smaller aortic arch lesions in diabetic $Ldlr^{-/-}$ mice, especially those devoid of *Ager*. *B*: $CD68^{+}$ macrophages were laser captured from aortic sinus atherosclerotic lesions of diabetic $Ldlr^{-/-}/Ager^{+/+}$ and $Ldlr^{-/-}/Ager^{-/-}$ mice, and mRNA transcript levels were determined for *Abca1*, *Abcg1*, and *Pparg* ($n = 6$ mice/group). Error bars represent mean ± SEM.

Table 1—Characteristics of diabetic *Ldlr*$^{-/-}$ and *Ldlr*$^{-/-}$/*Ager*$^{-/-}$ mice: plasma analyses

	Ldlr$^{-/-}$	*Ldlr*$^{-/-}$/*Ager*$^{-/-}$
Glucose (mg/dL)	322 ± 16.26	322 ± 16.24
HDL (mg/dL)	74 ± 11.12	84 ± 12.26*
TC (mg/dL)	1,524 ± 2.5	1,453 ± 1.9
TG (mg/dL)	274 ± 29.45	301 ± 24.27

Data are mean ± SEM. Glycemia, HDL, total cholesterol (TC), and triglyceride (TG) levels were obtained at kill after 15 weeks on a Western diet and after 2 months of hyperglycemia induced by STZ (n = 6). *$P < 0.05$ vs. *Ldlr*$^{-/-}$ mice.

and *Pparg* were significantly higher than those observed in WT HFD-fed mice (Supplementary Fig. 7*A–C*).

DISCUSSION

Hyperglycemia, pathognomonic of all forms of diabetes, leads to the generation of irreversibly formed AGEs. AGEs such as CML-AGE, a specific signaling ligand of RAGE (34), accumulate in hyperglycemia, and their production is exacerbated by inflammation and oxidative stress (42). Previous work has suggested that CML-AGE reduces HDL-mediated cellular cholesterol efflux (43); agents known to reduce levels of CML-AGE, aminoguanidine and metformin, prevented the suppressive effects of CML-AGE on reduction of HDL-mediated cellular cholesterol efflux. These data support modulatory roles for AGEs in the regulation of cholesterol efflux capacity. Here, we illustrate that these mechanisms depend on RAGE.

The current findings uncover important roles for PPARG in the mechanisms of CML-AGE/RAGE–dependent reduction in expression of *ABCA1* and *ABCG1*. Although PPARG agonists may exert their effects at least partly through downregulation of *Ager* (44,45), the present findings suggest that the converse is also true; that is, RAGE ligands directly suppress PPARG through ERK signal transduction. Previous work has suggested that CML-AGE reduces PPARG expression in chondrocytes (40); the current study illustrates new roles for AGE/RAGE in the suppression of PPARG in macrophages and suggests a potential novel role for the AGE/RAGE pathway in distinct effects of PPARG, such as macrophage polarization (37–39). Indeed, preliminary findings reveal that *Ager*$^{-/-}$ BMDMs (nondiabetic or diabetic) display increased levels of prototypic M2 markers versus WT BMDMs (data not shown).

The current work suggests that the CML-AGE/RAGE axis suppresses *ABCA1* and *ABCG1* promoter luciferase activity and transcription through elements in the human *ABCA1* and *ABCG1* promoters containing PPRE but not LXR-dependent elements. Consistent with this concept, the present data reveal that CML-AGE imparts no suppressive effect on *ABCA1* or *ABCG1* promoter luciferase activity as stimulated by the LXR agonist T0901317. Ozasa et al. (46) previously reported that the PPARG agonist pioglitazone enhances cholesterol efflux through regulation of ABCA1 and ABCG1. They showed that LXR contributed to the effects of pioglitazone transactivation of *ABCA1* but was only partially involved in the regulation of *ABCG1*. The current experimental strategy specifically testing the effect of CML-AGE/RAGE suggests that the suppressive effects of this axis were LXR independent/PPARG dependent. Precedent for LXRa/LXRb–independent regulation of *Abcg1* was previously demonstrated in mice in which PPARG agonism stimulated regulation of *Abcg1* in mice devoid of both *Nrlh3* and *Nrlh2* (47).

The current studies reveal that deletion of *Ager* in diabetic mice results in higher levels of plasma HDL and reduced total cholesterol. Although the higher expression of *Abca1* and *Abcg1* in *Ager*$^{-/-}$ diabetic BMDMs versus WT would not be expected to increase plasma levels of HDL (48), the present data revealing *Ager* deletion–dependent significant increases in hepatic ABCA1 protein suggest a plausible mechanism for these observations. It was recently proposed that a greater understanding of HDL function through its action on promotion of cholesterol efflux and RCT might be more clinically relevant than the absolute levels of HDL (49). More in-depth analysis of specific cholesterol components and potential modulatory roles for RAGE will be beneficial to fully understanding the reduced total cholesterol levels observed in *Ager*$^{-/-}$ mice. We suggest that despite the present findings that the beneficial effects of blockade/deletion of *Ager* are largely limited to the diabetic state, especially in an atherosclerosis context, these results nevertheless are meaningful because accelerated macrovascular disease is a major cause of morbidity and mortality in subjects with diabetes. It is important to note that beyond macrophages, studies have shown key roles for the endothelium, particularly with respect to LXR biology, in the pathogenesis of atherosclerosis (50). We conclude that because large-scale clinical trials indicate that the benefits of statins in regression of atherosclerosis in subjects with diabetes may be less prominent than those in subjects without diabetes (51,52), the present work may fill an important therapeutic gap in diabetic cardiovascular disease.

Acknowledgments. The authors gratefully acknowledge the expert assistance of Latoya Woods of the Diabetes Research Program, Department of Medicine, NYU School of Medicine, in the preparation of this manuscript. They also thank the members of the NYU Histology Core; Edward Fisher and Hitoo Nishi of the Department of Medicine, NYU School of Medicine, for expert assistance with LCM; and Alan Tall and Tamara Pagler of the Department of Medicine, Columbia University Medical Center, for expert assistance with the cholesterol efflux assay.

Funding. These studies were supported by grants from the U.S. Public Health Service (HL60901 and HL118565). The NYU Histology Core is partially supported by NYU Cancer Institute Cancer Center Support Grant 5P30CA016087-31.

Duality of Interest. No potential conflicts of interest relevant to this article were reported.

Author Contributions. G.D. and X.S. codesigned the experiments, performed the research, analyzed the data, and contributed to the writing of the manuscript. L.S., D.T., A.A., C.H.d.P., R.Ro., and F.S. performed the research and

reviewed the manuscript. R.A.F. and R.Ra. contributed to the experimental design of the research, analyzed the data, and reviewed and edited the manuscript. A.M.S. designed the experiments, reviewed data and the analysis, and wrote and edited the manuscript. A.M.S. is the guarantor of this work and, as such, had full access to all of the data in the study and takes responsibility for the integrity of the data and the accuracy of the data analysis.

References

1. Laing SP, Swerdlow AJ, Slater SD, et al. Mortality from heart disease in a cohort of 23,000 patients with insulin-treated diabetes. Diabetologia 2003; 46:760–765
2. Panzram G. Mortality and survival in type 2 (non-insulin-dependent) diabetes mellitus. Diabetologia 1987;30:123–131
3. Burke AP, Kolodgie FD, Zieske A, et al. Morphologic findings of coronary atherosclerotic plaques in diabetics: a postmortem study. Arterioscler Thromb Vasc Biol 2004;24:1266–1271
4. Shiu SW, Zhou H, Wong Y, Tan KC. Endothelial lipase and reverse cholesterol transport in type 2 diabetes mellitus. J Diabetes Investig 2010;1:111–116
5. Zhou H, Shiu SW, Wong Y, Tan KC. Impaired serum capacity to induce cholesterol efflux is associated with endothelial dysfunction in type 2 diabetes mellitus. Diab Vasc Dis Res 2009;6:238–243
6. de Boer JF, Annema W, Schreurs M, et al. Type I diabetes mellitus decreases in vivo macrophage-to-feces reverse cholesterol transport despite increased biliary sterol secretion in mice. J Lipid Res 2012;53:348–357
7. Khera AV, Cuchel M, de la Llera-Moya M, et al. Cholesterol efflux capacity, high-density lipoprotein function, and atherosclerosis. N Engl J Med 2011;364: 127–135
8. Rohatgi A, Khera A, Berry JD, et al. HDL cholesterol efflux capacity and incident cardiovascular events. N Engl J Med 2014;371:2383–2393
9. Mauldin JP, Nagelin MH, Wojcik AJ, et al. Reduced expression of ATP-binding cassette transporter G1 increases cholesterol accumulation in macrophages of patients with type 2 diabetes mellitus. Circulation 2008;117: 2785–2792
10. Patel DC, Albrecht C, Pavitt D, et al. Type 2 diabetes is associated with reduced ATP-binding cassette transporter A1 gene expression, protein and function. PLoS One 2011;6:e22142
11. Cipollone F, Iezzi A, Fazia M, et al. The receptor RAGE as a progression factor amplifying arachidonate-dependent inflammatory and proteolytic response in human atherosclerotic plaques: role of glycemic control. Circulation 2003;108: 1070–1077
12. Bu DX, Rai V, Shen X, et al. Activation of the ROCK1 branch of the transforming growth factor-beta pathway contributes to RAGE-dependent acceleration of atherosclerosis in diabetic apoE-null mice. Circ Res 2010;106: 1040–1051
13. Park L, Raman KG, Lee KJ, et al. Suppression of accelerated diabetic atherosclerosis by the soluble receptor for advanced glycation endproducts. Nat Med 1998;4:1025–1031
14. Morris-Rosenfeld S, Blessing E, Preusch MR, et al. Deletion of bone marrow-derived receptor for advanced glycation end products inhibits atherosclerotic plaque progression. Eur J Clin Invest 2011;41:1164–1171
15. Wendt T, Harja E, Bucciarelli L, et al. RAGE modulates vascular inflammation and atherosclerosis in a murine model of type 2 diabetes. Atherosclerosis 2006;185:70–77
16. Weischenfeldt J, Porse B. Bone marrow-derived macrophages (BMM): isolation and applications. CSH Protoc 2008;2008:pdb prot5080
17. Zhang X, Goncalves R, Mosser DM. The isolation and characterization of murine macrophages. Curr Protoc Immunol 2008;Chapter 14:Unit 14.1
18. Uehara Y, Miura S, von Eckardstein A, et al. Unsaturated fatty acids suppress the expression of the ATP-binding cassette transporter G1 (ABCG1) and ABCA1 genes via an LXR/RXR responsive element. Atherosclerosis 2007; 191:11–21
19. Matys V, Kel-Margoulis OV, Fricke E, et al. TRANSFAC and its module TRANSCompel: transcriptional gene regulation in eukaryotes. Nucleic Acids Res 2006;34:D108–D110
20. Kel-Margoulis OV, Tchekmenev D, Kel AE, et al. Composition-sensitive analysis of the human genome for regulatory signals. In Silico Biol 2003;3:145–171
21. Okuno M, Arimoto E, Ikenobu Y, Nishihara T, Imagawa M. Dual DNA-binding specificity of peroxisome-proliferator-activated receptor gamma controlled by heterodimer formation with retinoid X receptor alpha. Biochem J 2001;353:193–198
22. Lemberger T, Desvergne B, Wahli W. Peroxisome proliferator-activated receptors: a nuclear receptor signaling pathway in lipid physiology. Annu Rev Cell Dev Biol 1996;12:335–363
23. Srivastava S, Vladykovskaya E, Barski OA, et al. Aldose reductase protects against early atherosclerotic lesion formation in apolipoprotein E-null mice. Circ Res 2009;105:793–802
24. Zhang Y, Zanotti I, Reilly MP, Glick JM, Rothblat GH, Rader DJ. Overexpression of apolipoprotein A-I promotes reverse transport of cholesterol from macrophages to feces in vivo. Circulation 2003;108:661–663
25. Fligner MA, Killeen TJ. Distribution-free two sample tests of scale. J Am Stat Assoc 1976;75:315–319
26. Welch BL. On the comparison of several mean values: an alternative approach. Biometrika 1951;38:330–336
27. Westfall PH. Multiple testing of general contrasts using logical constraints and conditions. J Am Stat Assoc 1997;92:299–306
28. Westfall PH, Tobias RD. Multiple testing of general contrasts: truncated closure and the extended Shaffer-Royen method. J Am Stat Assoc 2007;102: 487–494
29. Hothorn T, Bretz F, Westfall P. Simultaneous inference in general parametric models. Biom J 2008;50:346–363
30. Zeiles A. Econometric computing with HC and HAC covariance matrix estimators. J Stat Softw 2006;11:1–17
31. Zeileis A. Object-oriented computation of sandwich estimators. J Stat Softw 2006;16:1–16
32. Mauldin JP, Srinivasan S, Mulya A, et al. Reduction in ABCG1 in type 2 diabetic mice increases macrophage foam cell formation. J Biol Chem 2006;281: 21216–21224
33. Tang C, Kanter JE, Bornfeldt KE, Leboeuf RC, Oram JF. Diabetes reduces the cholesterol exporter ABCA1 in mouse macrophages and kidneys. J Lipid Res 2010;51:1719–1728
34. Kislinger T, Fu C, Huber B, et al. N(epsilon)-(carboxymethyl)lysine adducts of proteins are ligands for receptor for advanced glycation end products that activate cell signaling pathways and modulate gene expression. J Biol Chem 1999; 274:31740–31749
35. Boisvert WA, Black AS, Curtiss LK. ApoA1 reduces free cholesterol accumulation in atherosclerotic lesions of apoE-deficient mice transplanted with apoE-expressing macrophages. Arterioscler Thromb Vasc Biol 1999;19: 525–530
36. Tontonoz P, Mangelsdorf DJ. Liver X receptor signaling pathways in cardiovascular disease. Mol Endocrinol 2003;17:985–993
37. Chawla A, Barak Y, Nagy L, Liao D, Tontonoz P, Evans RM. PPAR-gamma dependent and independent effects on macrophage-gene expression in lipid metabolism and inflammation. Nat Med 2001;7:48–52
38. Chawla A, Boisvert WA, Lee CH, et al. A PPAR gamma-LXR-ABCA1 pathway in macrophages is involved in cholesterol efflux and atherogenesis. Mol Cell 2001;7:161–171
39. Moore KJ, Rosen ED, Fitzgerald ML, et al. The role of PPAR-gamma in macrophage differentiation and cholesterol uptake. Nat Med 2001;7:41–47
40. Yang Q, Chen C, Wu S, Zhang Y, Mao X, Wang W. Advanced glycation end products downregulates peroxisome proliferator-activated receptor γ expression in cultured rabbit chondrocyte through MAPK pathway. Eur J Pharmacol 2010; 649:108–114

41. Merat S, Casanada F, Sutphin M, Palinski W, Reaven PD. Western-type diets induce insulin resistance and hyperinsulinemia in LDL receptor-deficient mice but do not increase aortic atherosclerosis compared with normoinsulinemic mice in which similar plasma cholesterol levels are achieved by a fructose-rich diet. Arterioscler Thromb Vasc Biol 1999;19:1223–1230
42. Anderson MM, Requena JR, Crowley JR, Thorpe SR, Heinecke JW. The myeloperoxidase system of human phagocytes generates Nepsilon-(carboxymethyl)lysine on proteins: a mechanism for producing advanced glycation end products at sites of inflammation. J Clin Invest 1999;104:103–113
43. Machado AP, Pinto RS, Moysés ZP, Nakandakare ER, Quintão EC, Passarelli M. Aminoguanidine and metformin prevent the reduced rate of HDL-mediated cell cholesterol efflux induced by formation of advanced glycation end products. Int J Biochem Cell Biol 2006;38:392–403
44. Yang Y, Zhao LH, Huang B, et al. Pioglitazone, a PPARγ agonist, inhibits growth and invasion of human hepatocellular carcinoma via blockade of the rage signaling. Mol Carcinog. 12 October 2014 [Epub ahead of print]. DOI: 10.1002/mc.22231
45. Liang YJ, Jian JH, Chen CY, Hsu CY, Shih CY, Leu JG. L-165,041, troglitazone and their combination treatment to attenuate high glucose-induced receptor for advanced glycation end products (RAGE) expression. Eur J Pharmacol 2013;715:33–38
46. Ozasa H, Ayaori M, Iizuka M, et al. Pioglitazone enhances cholesterol efflux from macrophages by increasing ABCA1/ABCG1 expressions via PPARγ/LXRα pathway: findings from in vitro and ex vivo studies. Atherosclerosis 2011;219:141–150
47. Li AC, Binder CJ, Gutierrez A, et al. Differential inhibition of macrophage foam-cell formation and atherosclerosis in mice by PPARalpha, beta/delta, and gamma. J Clin Invest 2004;114:1564–1576
48. Rader DJ, Alexander ET, Weibel GL, Billheimer J, Rothblat GH. The role of reverse cholesterol transport in animals and humans and relationship to atherosclerosis. J Lipid Res 2009;50(Suppl.):S189–S194
49. Tuteja S, Rader DJ. High-density lipoproteins in the prevention of cardiovascular disease: changing the paradigm. Clin Pharmacol Ther 2014;96:48–56
50. Hayashi T, Kotani H, Yamaguchi T, et al. Endothelial cellular senescence is inhibited by liver X receptor activation with an additional mechanism for its atheroprotection in diabetes. Proc Natl Acad Sci U S A 2014;111:1168–1173
51. Neeli H, Gadi R, Rader DJ. Managing diabetic dyslipidemia: beyond statin therapy. Curr Diab Rep 2009;9:11–17
52. Stegman B, Puri R, Cho L, et al. High-intensity statin therapy alters the natural history of diabetic coronary atherosclerosis: insights from SATURN. Diabetes Care 2014;37:3114–3120